

CONDENSED MATTER PHYSICS

Stable vortices in the anomalous metallic state observed on monoatomic-layer superconductors

Yudai Sato^{1,2,3*}, Masahiro Haze¹, Ryohei Nemoto⁴, Wenxuan Qian^{4,5}, Shunsuke Yoshizawa⁶, Takashi Uchihashi^{4,5}, Yukio Hasegawa¹

The superconductor-insulator transition in two-dimensional (2D) systems has been extensively studied as a typical example of quantum phase transition. Recent investigations of highly conductive 2D systems have revealed an intervening metallic regime, in which the electrical resistivity saturates at the limit of zero temperature. The nature and origin of this metallicity remain debated, partly because of the lack of microscopic understanding. In this study, using scanning tunneling spectroscopy, we investigate the metallic state and other phases observed in crystalline Pb monoatomic-layer superconductors formed on vicinal semiconducting substrates. Our spectroscopic images reveal stable and isolated vortices in the metallic regime, distinct from delocalized or liquidized vortices. These findings suggest that the saturated resistance in the metallic state arises from the pinning-free vortex motion driven by the finite current applied for the transport measurements. Our disorder-controlled microscopic experiments provide new insights into the fluctuation-induced phases of ultrathin crystalline 2D superconductors.

INTRODUCTION

Recent technical progress has enabled the fabrication of atomically thin two-dimensional (2D) superconducting systems, such as superconducting interface (1–5), atomic sheets of transition metal dichalcogenides (6–8), and metal atomic layers on semiconductor surfaces (9–17), to reinvestigate exotic superconducting properties in a more controlled manner than previously achieved. One of the unique phenomena in 2D superconductors is a superconductor-insulator transition (SIT) that occurs at the limit of zero temperature (18–28) by introducing disorder (18, 23, 27), applying perpendicular magnetic fields (21, 24), and reducing thickness (19, 20, 22, 24–26). As a typical example of quantum phase transitions, SIT has been extensively studied in various 2D electron systems, including amorphous or granular thin films (18–25, 27) and Josephson junction arrays (29, 30).

According to conventional theory (31), SIT is driven by the localization of Cooper pairs thorough the phase fluctuation of the superconducting order parameter. The theory predicts that the transition occurs when a sheet resistance R_s is around the quantum resistance R_Q for Cooper pairs ($\equiv h/4e^2 = 6.45$ k Ω , where h is the Planck constant, and e is the electron charge). It is believed that SIT occurs directly from the superconductor to the insulator without any intervening phases. Unexpectedly, however, investigations of SIT on less disordered systems or atomically thin superconductors, which exhibit normal sheet resistance R_N less than R_Q , have revealed the presence of an intervening metallic regime called the anomalous metallic (AM) state (4, 5, 7, 8, 14, 32–43). The AM state is characterized by a saturated finite resistance, which is lower than R_N at the limit of zero temperature.

The origin of the AM state has been debated (4, 34, 36, 37, 42–49), and some claim that it is due to delocalized vortices induced by quantum fluctuations (QFs) (4, 34, 36, 42, 44–46). However, this remains unresolved, in part because of the lack of microscopic investigations.

Previous SIT experiments on 2D superconducting systems primarily used macroscopic methods (e.g., electron and heat transport) (4, 5, 8, 14, 18–27, 29, 30, 32–34, 36, 38–43). Although several microscopic studies on SIT using scanning tunneling microscopy and spectroscopy (STM/S) have been reported, their targets have been limited to highly disordered amorphous thin films (50–52). Therefore, a microscopic investigation of SIT using STM/S on highly conductive and crystalline 2D superconductors, which may exhibit an AM state with precise control of the disorder, is desired.

Here, we report the magnetic field-induced SIT of superconducting Pb monoatomic layers formed on flat and vicinal Si(111) substrates, where the surface steps act as controllable sources of disorder. We first identified the range of magnetic fields that exhibit the AM state in electrical transport measurements. Using STM, we obtained spectroscopic images showing the spatial distribution of tunneling conductance at the bottom of the superconducting gap [zero-bias conductance (ZBC)] and observed stable and isolated vortices under magnetic fields that correspond to the AM state, where stable vortices mean the ones not moving during STM observation. The ZBC maps taken in the AM state are clearly different from those taken in higher magnetic fields, where the enhanced ZBC is distributed over the entire surface, presumably owing to delocalized vortices. Our observation of stable and isolated vortices contradicts the model of a quantum vortex liquid (VL), in which vortices are supposed to be mobile owing to QFs. Instead, our results suggest that the pinning-free mobile vortices driven by the current applied for the transport measurements are responsible for the AM state. In addition, we investigated the role of disorder in the emergence of various states by controlling the step density through the adjustment of the miscut angle of the vicinal substrate. We observed a state exhibiting metallic temperature dependence above the critical magnetic field on the flat sample and found that the state transitions into an insulating state upon the introduction of the disorder.

¹The Institute for Solid State Physics, The University of Tokyo, 5-1-5 Kashiwa-no-ha, Kashiwa 277-8581, Japan. ²Leiden Institute of Physics, Leiden University, Niels Bohrweg 2, 2333 CA Leiden, Netherlands. ³Faculty of Physics, Ludwig Maximilian University of Munich, Geschwister-Scholl-Platz 1, 80539 Munich, Germany. ⁴Research Centre for Materials Nanoarchitectonics (MANA), National Institute for Materials Science, 1-1 Namiki, Tsukuba 305-0044, Japan. ⁵Graduate School of Science, Hokkaido University, Kita-10 Nishi-8, Kita-ku, Sapporo 060-0810, Japan. ⁶Center for Basic Research on Materials, National Institute for Materials Science, 1-2-1 Sengen, Tsukuba 305-0047, Japan.

*Corresponding author. Email: yudai.sato@lmu.de

RESULTS

Superconductivity of atomically thin 2D crystalline layers

The highly crystalline 2D superconductor investigated in this study is a striped incommensurate (SIC) phase of monolayer Pb formed on Si(111) substrates (9–11, 15–17, 53, 54). We used flat and vicinal substrates tilted from the (111) orientation by 0.5° and 1.1° , respectively, to introduce surface steps. The temperature (T)-dependent R_s measured at zero magnetic field ($B = 0$), presented in Fig. 1A, exhibits a superconducting transition of the SIC phases formed on flat and 1.1° substrates at critical temperatures T_c of 1.53 and 1.21 K, respectively. T_c values were estimated by fitting with the 2D Aslamazov-Larkin and Maki-Thompson terms (55, 56), as shown in fig. S3 (A and B) in the Supplementary Materials. The reduction in T_c with the introduction of steps indicates that steps act as disorder and, in other words, a resistance for atomic metal layers (10, 15, 16, 57–59). It is noteworthy that R_s at $T > T_c$ was much lower than R_Q . The smeared onset of R_s also allowed us to estimate the Berezinskii-Kosterlitz-Thouless transition (60, 61) temperature T_{BKT} at 1.29 and 0.83 K for the flat and 1.1° samples, respectively (see fig. S3).

Figure 1B shows an STM image captured on a 1.1° -tilted vicinal SIC sample. Steps with a height of 0.31 nm are found at an average interval of 16.0 nm. This spacing is much shorter than the typical terrace width (~ 400 nm) and superconducting coherence length (~ 35 nm) of a flat sample. The inset shows an atomically resolved image of the SIC phase, revealing characteristic domain structures consisting of a local $\sqrt{3}$ -by- $\sqrt{3}$ -Pb structure with quasi- $\sqrt{7}$ -by- $\sqrt{3}$ -Pb boundaries (54). The tunneling conductance (dI/dV) spectra obtained by STM for both the flat (Fig. 1C) and vicinal (Fig. 1D) SIC samples exhibit a superconducting gap at $B = 0$ (black curves). Fitting the spectra using the Dynes function (62) yields gap sizes of 0.33 and 0.22 meV, respectively. The V-shaped dip observed in the dI/dV spectra taken at 2 T (red curves), which is much higher than the critical magnetic field B_{c2} (250 to 400 mT), is a zero-bias anomaly (ZBA) owing to Coulomb interactions enhanced by electron scattering (63, 64). This dip is common in 2D metal layers (see fig. S3) (13, 50, 65) and is enhanced by the disorder. Because the ZBA remains invariant under the relevant magnetic field range, its contribution can be eliminated by normalizing the spectra with

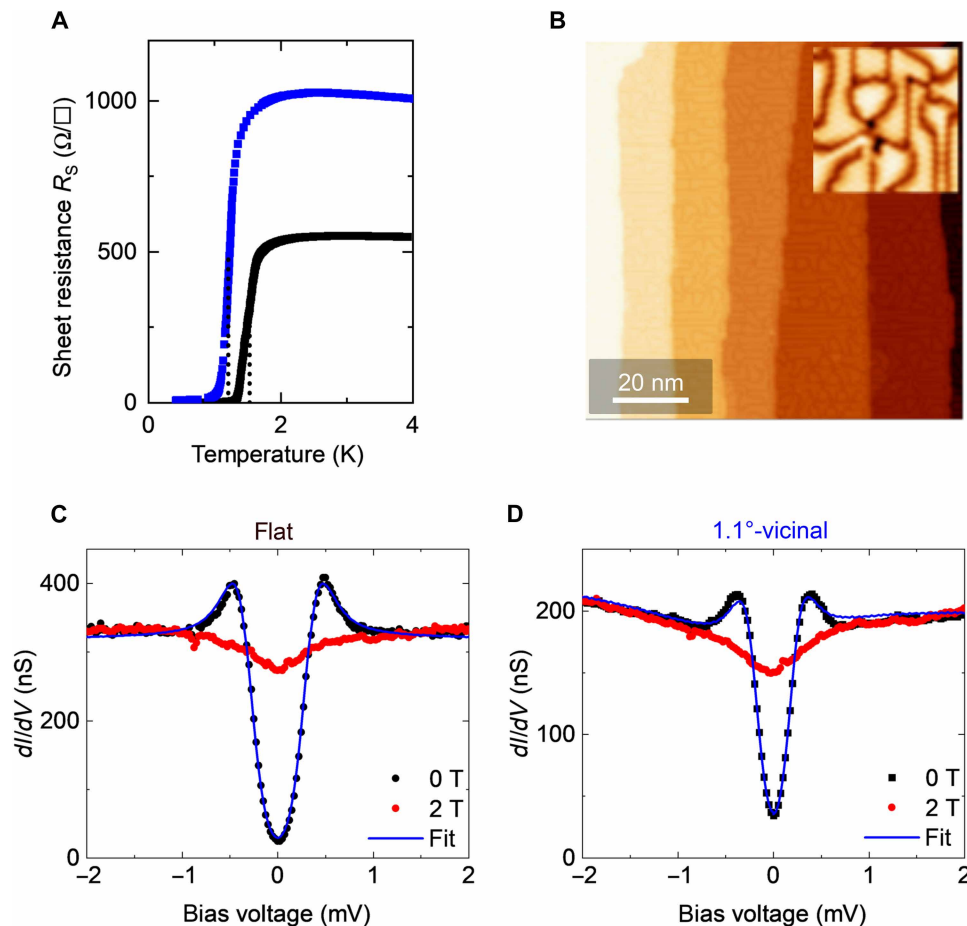


Fig. 1. Superconductivity of monoatomic-layer Pb layers formed on flat and 1.1° -vicinal Si(111) substrates. (A) Temperature dependence of the sheet resistance R_s of flat (black curve) and 1.1° -vicinal (blue curve) SIC samples under a zero magnetic field. (B) STM image of the SIC phase formed on a 1.1° -tilted vicinal Si(111) sample. The inset shows a magnified image (sample bias voltage $V_s = 1$ V and tunneling current $I_t = 20$ pA). (C and D) Tunneling conductance (dI/dV) spectra taken at $T = 0.36$ K on (C) the flat and (D) 1.1° -vicinal samples under the out-of-plane magnetic field of 0 T (black circles) and 2 T (red circles), respectively. The tip was stabilized at $V_s = 2.2$ mV and $I_t = 400$ pA. The blue line indicates a fitted Dynes function with parameters of a superconducting gap Δ , the pair-breaking parameter Γ , and effective temperature T_{eff} ($\Delta = 0.33$ meV, $\Gamma = 2$ μ eV, and $T_{\text{eff}} = 0.97$ K for the flat sample; $\Delta = 0.22$ meV, $\Gamma = 2$ μ eV, and $T_{\text{eff}} = 0.85$ K for the vicinal sample). The fitting was performed after normalizing the spectra to those obtained at 2 T.

those obtained at a magnetic field above B_{c2} . The value of $2\Delta/k_B T_c$ for the vicinal sample (5.0) is larger than that of the flat sample (4.2). The increase in $2\Delta/k_B T_c$ can be understood as follows: The reduced T_c of the vicinal sample is mainly due to the suppression of the superconducting phase coherence, while Δ and the Cooper pairs are not suppressed in comparison with the phase (66). This suggests an important role for the steps in the breaking of phase coherence, which leads to the decoherence and localization of Cooper pairs.

AM states in SIT

We then performed transport measurements under an out-of-plane magnetic field B . Figure 2A displays the R_s - T curves obtained for the 1.1° -tilted vicinal sample under various magnetic fields. At $B = 0$, R_s decreases to zero, and the sample becomes a superconductor at low temperatures. However, in the range of $25 \text{ mT} < B < 100 \text{ mT}$, R_s exhibits saturating behavior near $T = 0$, indicating the presence of finite resistance in the limit of $T = 0$, that is, an AM state (4, 5, 7, 8, 14, 33, 34, 36–41, 43). Near $T = 0$, R_s increases with T ($dR/dT > 0$); that is, R_s exhibits metallic temperature dependence below $B = 200 \text{ mT}$. Subsequently, the temperature dependence switches to insulating ($dR/dT < 0$) at approximately $B = 300 \text{ mT}$. A similar SIT with intervening metallic states was observed in the flat sample (see fig. S4B).

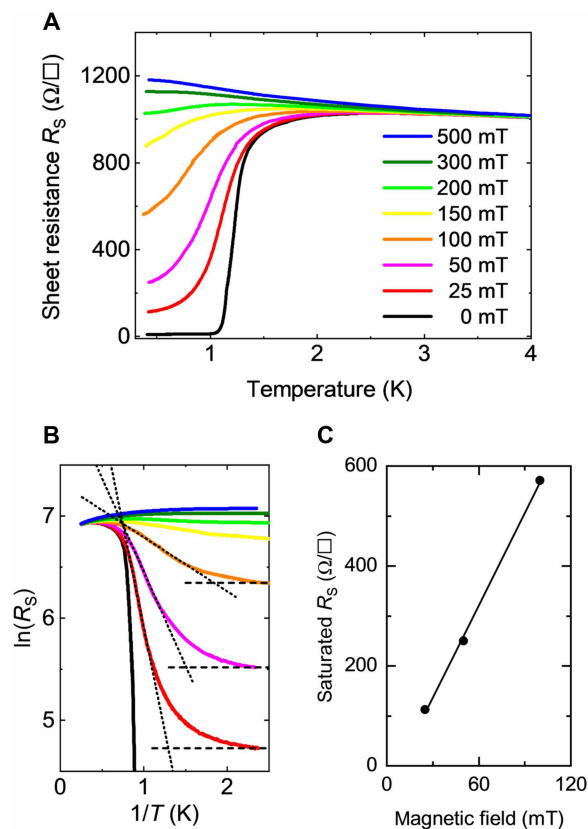


Fig. 2. Surface electron transport measurements under out-of-plane magnetic fields. (A) Temperature dependence of R_s for the 1.1° -vicinal SIC sample under out-of-plane magnetic fields. (B) Arrhenius plots of (A). The dotted lines correspond to the resistance resulting from the thermally activated vortex motion, and the dashed lines are the saturated resistances at low temperatures. (C) Saturated resistance as a function of the magnetic field.

In the Arrhenius plot (Fig. 2B), the temperature-independent portion (dashed line) represents the AM state. The linearly increasing part (dotted line) corresponds to the thermally activated motion of the vortices (67), described by $R_s \propto \exp[-U(B)/k_B T]$, where $U(B)$ is the magnetic field-dependent potential barrier for the vortex motion, and k_B is the Boltzmann constant (see text S4 in the Supplementary Materials). The crossover temperature, T_{cross} , was determined as the crossing point of the dashed and solid lines for each magnetic field.

STM on AM states

After confirming the presence of the AM state through transport measurements, we performed STM for microscopic elucidation to reveal the behavior of the vortices. Figure 3 (B to P) shows a series of ZBC maps taken on a 1.1° -tilted vicinal sample at 0.36 K on the same area as the STM image of Fig. 3A under various magnetic fields.

In the ZBC image of $B = 30 \text{ mT}$ (Fig. 3C), an oval-shaped vortex was observed and different from the round vortex observed on the flat sample (fig. S6). These elongated vortices are called Abrikosov-Josephson vortices because of the limited critical current density across high-density steps (12, 16, 28). Despite the presence of steps, the vortices maintain an intrinsic triangular-lattice arrangement as shown in Fig. 3 (D to F), indicating that the pinning force is still weak compared with the intervortex interaction. Our previous work indicated that in the SIC phase on the vicinal substrates, where the oval vortices are situated across approximately four steps on average, the pinning force at these steps is rather weak because of the very weak electronic disruption across each single step (16).

With an increase in B , the density of the vortices increased, which is consistent with that expected from the magnetic flux density (Fig. 3Q). However, at 120 mT (Fig. 3F) and above, the number of observed vortices, which is obtained by counting the local maxima in the ZBC images, is less than that expected, suggesting that some of the vortices are delocalized in the timescale of the STM scanning, as will be discussed later in detail. At 240 mT and above (Fig. 3, J to L), individual vortices are not resolved and the high ZBC area spreads over the surface, presumably owing to the liquidation of all the vortices (68). The flat sample also exhibits stable vortices and vortex liquidation, as shown in fig. S6. We note that the transition from the stable vortex to the delocalized vortex, and subsequently to the VL, cannot be detected in transport measurements, where the AM state appears.

According to the Arrhenius plot in Fig. 2B, at 0.36 K , where $1/T$ is 2.8 , the AM state appears under magnetic fields of $0 < B < 100 \text{ mT}$, where the ordered vortex state is observed by STM. In this regime, the saturated resistance increases proportionally with B , as shown in Fig. 2C, indicating that the resistance is proportional to the density of the vortices. This proportional relationship suggests that the resistance is due to the pinning-free motion of the vortices (4). The slope of saturated $R_s(B)$ ($6.4 \times 10^3 \Omega/\text{T}$) is larger than the expected value R_N/B_{c2} ($2.8 \times 10^3 \Omega/\text{T}$), as predicted by the Bardeen-Stephan model (69). This suggests that in the AM state, vortices move more diffusively than expected. This behavior is commonly observed in systems exhibiting the AM state (4, 8).

In the AM state, the vortices are stable under no lateral current flow, as observed by STM. However, they become mobile in a pinning-free manner under the current applied for transport measurements, presumably owing to weak vortex pinning. It is inconsistent with that of quantum fluctuation-induced vortex mobility. The extrinsic origin of the AM state we observed is in line with recent

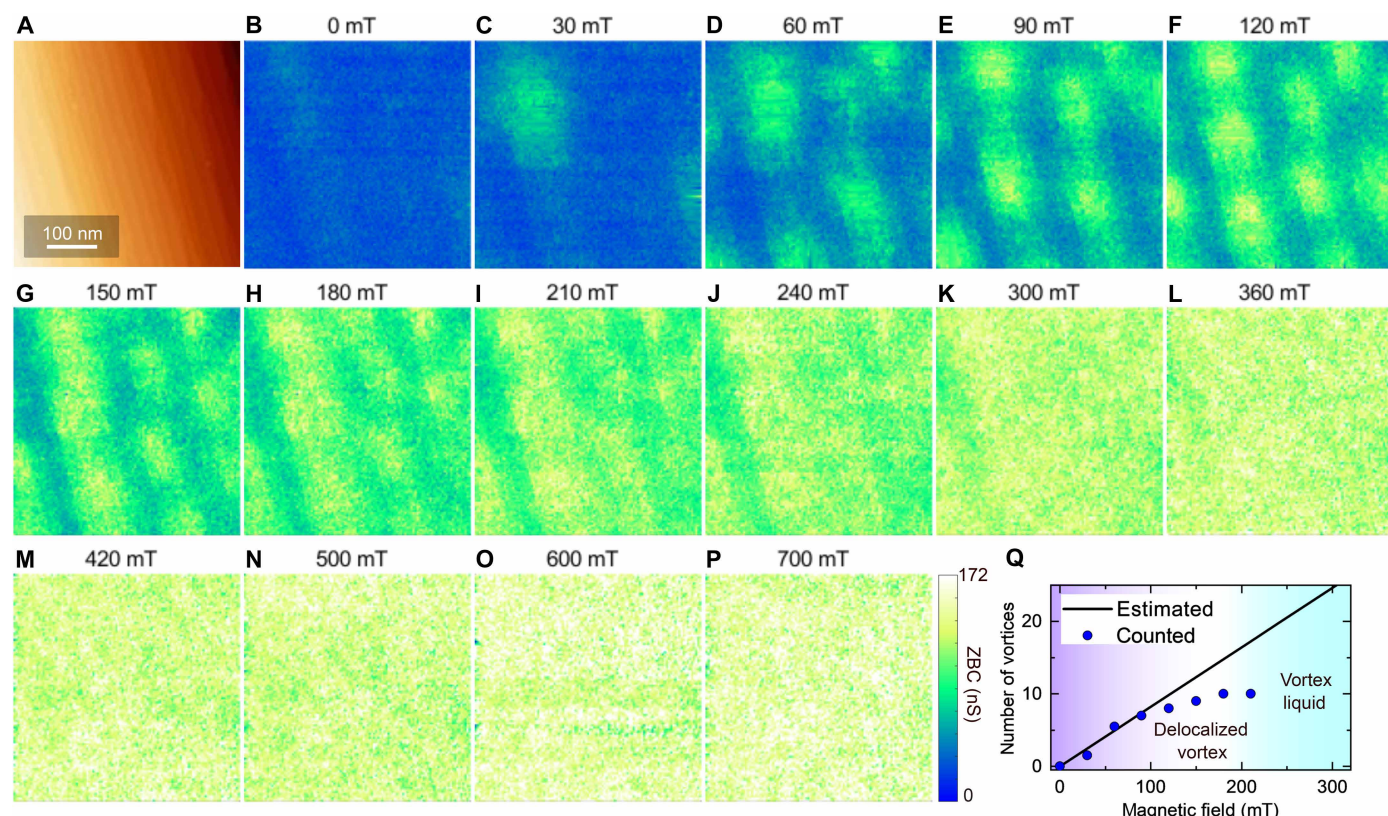


Fig. 3. STS measurements under out-of-plane magnetic fields. (A) STM image of the 1.1° -tilted vicinal sample. (B to P) ZBC maps under various out-of-plane magnetic fields obtained in the same area as (A) ($V_s = 2.2$ mV, $I_t = 400$ pA). (Q) Number of vortices as a function of magnetic field. The solid black line indicates the number of vortices estimated from the applied magnetic field.

reports that it is suppressed by the insertion of a radio frequency filter in transport measurements, where unintended ac components of the current induce the motion of weakly pinned vortices in 2D systems (41, 70–72).

As shown in Fig. 3Q, some vortices begin to delocalize at ~ 120 mT, and all of them are liquidized at ~ 240 mT. In the VL phase [240 to 360 mT; see Fig. 3 (I to L)], the superconducting gap remains and becomes shallower with the magnetic field because of the increase in the number of delocalized vortices.

In the 360-mT ZBC map (Fig. 3L), ZBC appears homogeneous over the entire area, indicating that the applied magnetic field is close to B_{c2} . We estimated B_{c2} from the evolution of ZBC as a function of B . In a plot of the peak value μ in the ZBC histogram obtained away from the vortex centers (Fig. 4B; see text S7 in the Supplementary Materials for details), one can see that μ increases linearly with B (solid lines). B_{c2} is obtained from the intersection of the solid line with the saturated value (dashed line) (9, 10). The obtained critical field, $B_{c2} = 344 \pm 6$ mT (red line), is consistent with that obtained from the transport measurement, as discussed later.

Above B_{c2} , the gap remains but is slowly suppressed with B and eventually disappears at ~ 600 mT. The magnetic field at which the gap disappears is denoted by $B^* = 552 \pm 34$ mT, as indicated by the green line in Fig. 4B. Figure 4D shows the color-coded dI/dV spectra normalized by the spectrum taken at 2 T of the vicinal sample under various magnetic fields. The blue region around 0 T corresponds to the superconducting gap. Above B_{c2} (red line), the gap

remains, albeit with no coherence peaks. Last, the gap disappears completely at B^* . The observed gaps are similar to a pseudogap reported for MoGe amorphous thin films (52); thus, we attributed the gap to phase-incoherent Cooper pairs induced by the phase fluctuations following the interpretation of a previous study (38). We note that we could see no distinct features corresponding to B^* in transport measurements.

B-T phase diagram in transport properties

B_{c2} 's and phases above the fields were investigated using transport measurements. To estimate B_{c2} , we applied the Ullah-Dorsey (UD) scaling theory (73) at $T > T_c/2$, as described in fig. S5D. The obtained B_{c2} 's are plotted in the B - T phase diagrams of the vicinal samples in Fig. 5D. The Werthamer-Helfand-Hohenberg (WHH) theory (74) is used to evaluate $B_{c2}(T)$ at $T < T_c/2$ (dashed curve). B_{c2} obtained by STM at $T = 0.36$ K (344 ± 6 mT), marked with a black square, is consistent with the WHH curve.

Above B_{c2} , we define the superconducting onset temperature T_{onset} as the boundary between the regions with metallic ($dR/dT > 0$) and insulating ($dR/dT < 0$) temperature dependencies, corresponding to the temperature at which $dR/dT = 0$, as shown in Fig. 5A. To see the boundary in the lower temperature side, we took the cross-point B_{cross} of the two R_s - B curves obtained at the nearest temperature, which is equivalent to the magnetic field at T_{onset} (5). B_{cross} is indicated by the dots in Fig. 5B. The obtained T_{onset} and B_{cross} data points are plotted in the phase diagram. The same analyses were

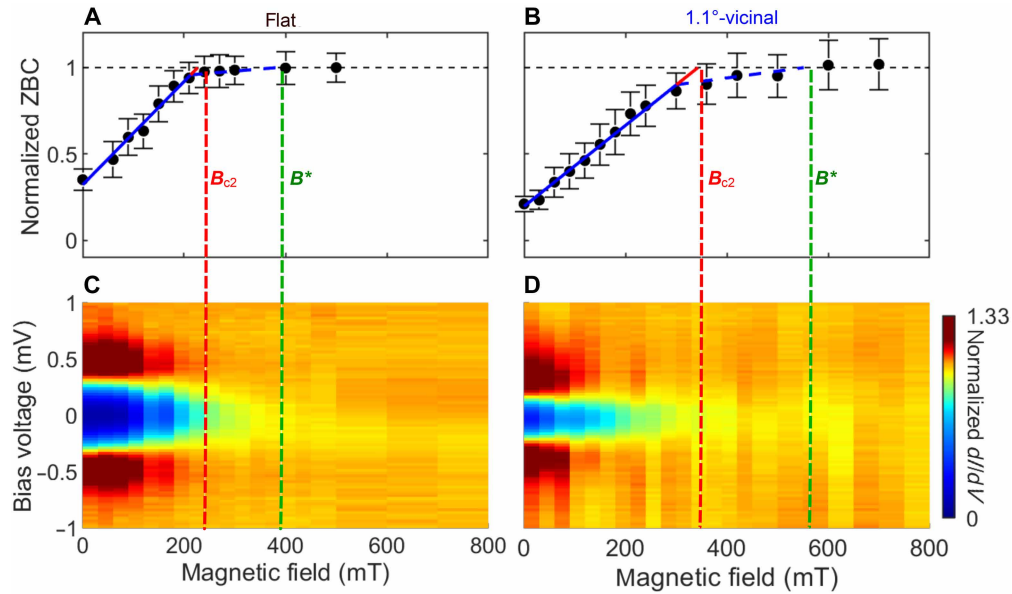


Fig. 4. Gap closure using magnetic fields. (A and B) Normalized ZBC values as a function of the magnetic field for (A) flat and (B) 1.1°-vicinal samples. The red and green lines correspond to the upper critical magnetic field B_{c2} and the field at which the pseudogap disappears B^* , respectively. The dataset used for analysis is shown in fig. S6 and Fig. 3. (C and D) Color-coded differential conductance (dI/dV) spectra under various magnetic fields taken on (C) flat ($V_S = 9.2$ mV, $I_T = 200$ pA) and (D) 1.1°-vicinal samples ($V_S = 2.2$ mV, $I_T = 400$ pA). The values were normalized by the conductance under 500 mT for the flat sample (18 nS) and under 2 T for the 1.1°-vicinal sample (143 nS).

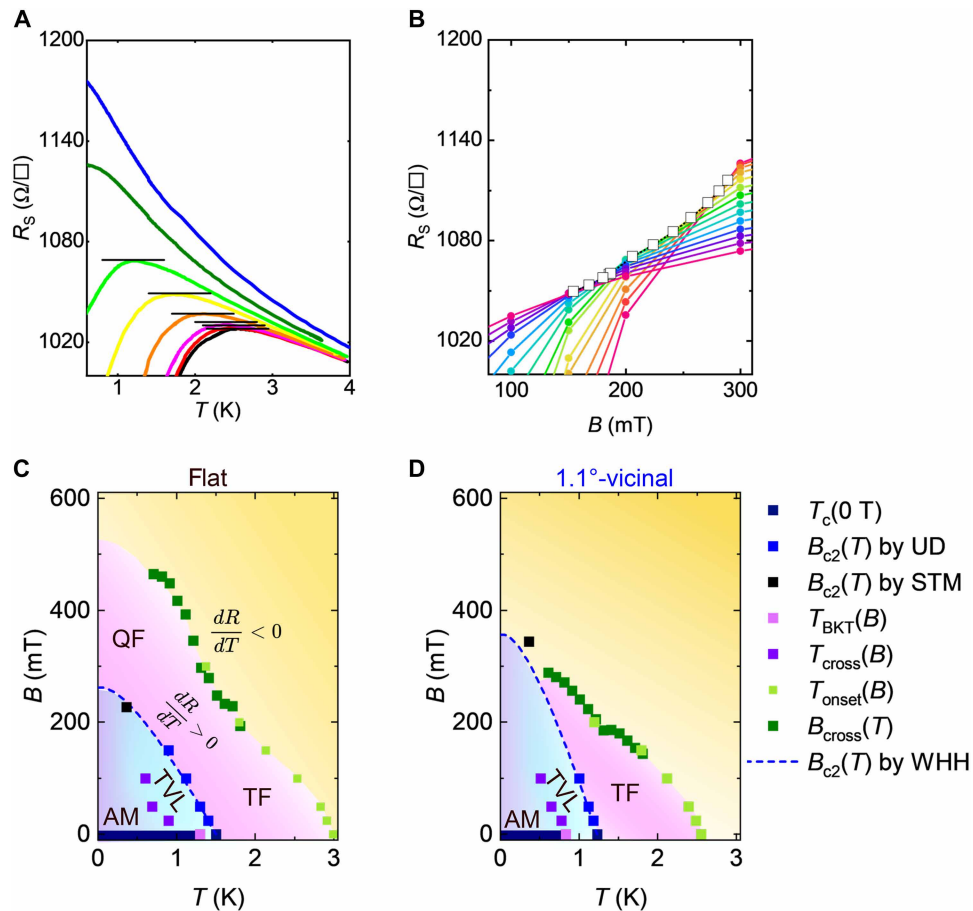


Fig. 5. B - T phase diagrams of flat and vicinal samples. (A) Zoomed-in plots of R_s - T curves in Fig. 2A around points with $dR_s/dT = 0$. (B) R_s - B curves taken at various temperatures from 0.56 to 1.86 K with an increment of 0.1 K. Crossing points B_{cross} , open circles. (C and D) B - T phase diagrams of the flat and 1.1°-vicinal samples. S, superconductors; AM, anomalous.

performed for the flat sample [see figs. S4 (B to D) and S5 (A to C)] and are presented in Fig. 5C.

We first examine the region below $B_{c2}(T)$ in the phase diagrams. Near $B = 0$, R_s is zero when $T < T_{\text{BKT}}$. This area is defined as the superconducting phase (S). The area where $R_s \neq 0$ can be separated into two regimes by T_{cross} : The region where $T < T_{\text{cross}}$ is the AM state, and the remaining $T > T_{\text{cross}}$ region is the thermally activated VL phase (TVL). In $B > B_{c2}(T)$, the superconducting onset curve by T_{onset} (light green squares) and B_{cross} (green) divides the area into two regions with metallic (pinkish) and insulating (orange) temperature dependences. The metallicity outside the $B_{c2}(T)$ curve is due to the formation of Cooper pairs induced by fluctuations. The region near $B = 0$ corresponds to the paraconductivity induced by thermal fluctuation (TF) (55, 56). In the case of the flat sample, the metallic region extends further than that of the vicinal sample, reaching zero temperature above $B_{c2}(T)$. Because the TF is suppressed in the limit of $T = 0$, the metallic part near $T = 0$ likely originates from QF. A similar metallic phase was observed in previous studies of slightly disordered systems and was attributed to the quantum Griffith state (QGS) (5, 75). It is believed that in the QGS, rare regions that are locally superconducting persist in normal metals by QF. Although the divergent behavior of the critical exponent, one of the characteristic features of the QGS, was not confirmed in our measurement, the multiple cross points in the R_s - B curves, another characteristic of QGS, can be seen in our flat sample (inset of fig. S4D). The observed multiple cross points are in marked contrast to the conventional SIT, where all the R_s - B curves cross at a single point (33). For the 1.1° -vicinal sample, the superconducting onset curve did not reach zero temperature. The disorder induced by the steps of the 1.1° -tilted vicinal sample prevents the QF phase, which is consistent with the fact that the QGS emerges only in slightly disordered systems (5, 75).

Disorder-dependent phase evolution

Combining all the results obtained by the transport and STM measurements, we created a phase diagram of magnetic field versus disorder at $T = 0.36$ K, as shown in Fig. 6. Here, we have added the STM results obtained for a 0.5° -tilted vicinal sample (fig. S8). The red and green dotted lines represent B_{c2} and B^* , respectively. The gradual increase in B_{c2} with disorder is due to the reduced coherence length induced by the presence of steps (16).

The region below B_{c2} (red line) is separated into the VL phase (light blue) and AM phase (purple). In the AM states, stable vortices were observed using STM. However, they were not observed in the VL phase. The VL phase spreads over a wider range of B on the disordered samples, which implies that the disorder promotes the liquidation of the vortices, as explained by disorder-induced phase fluctuation. It is consistent with previous studies that reported invisible vortices in thin superconducting films (50) and the enhancement of the VL phase by increasing the R_s of the superconducting films (76).

In the range of $B_{c2} < B < B^*$, a pseudogap due to fluctuation-induced Cooper pairs was observed in the tunneling spectra. In the transport measurements, this region is separated into two phases, metallic and insulating, depending on the degree of disorder. The insulating regime is due to the presence of localized pairs, whereas the metallic regime is due to nonlocalized but incoherent Cooper pairs. This implies that through the introduction of these steps, the system approaches that of the conventional SIT (31). These localized pairs disappear at B^* , where the superconducting amplitude vanishes. The

increase in B^* with disorder corresponds to a previous numerical investigation of the SIT (77), where the amplitude survives at higher B in the case of a highly disordered system. The persistent preformed pairs with disorder are understood by the same analogy of B_{c2} enhancement: the reduced size of the localized Cooper pairs.

DISCUSSION

Here, we present the results of both macroscopic (transport) and microscopic (STM) measurements of monoatomic-layer superconducting films on vicinal substrates to investigate magnetic field-driven and disorder-driven phase evolution. Our study focuses on the atomic-layer films as an ideal platform for probing the quantum phase transition of 2D superconductors, given their intrinsic lack of

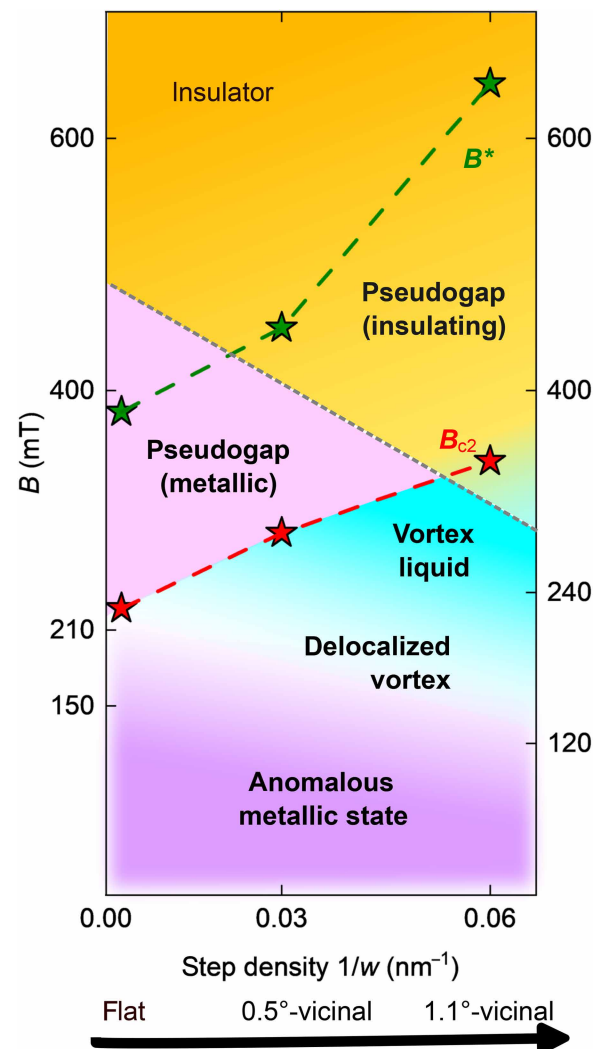


Fig. 6. Magnetic field-disorder (step density) diagram at $T = 0.36$ K. The phase diagram is obtained from the combined results of transport and STM measurements. Background colors indicate phases corresponding to the AM state (purple), metallic region (pink), and insulating region (orange) determined by transport measurements. The black dashed line represents the border between the metallic and insulating regions. The stars indicate the characteristic magnetic fields obtained from STM analysis: B_{c2} (red) and B^* (green).

disorder and ability to precisely control disorder by adjusting the miscut angle of the substrate without disturbing the crystal structures on terraces. Through a combination of macroscopic and microscopic measurements, we unveiled various unique phenomena in quantum phases. Notably, we found unexpected stable vortices in the regime of AM states, shedding light on the role of QFs in quantum phase transitions.

MATERIALS AND METHODS

Sample preparation

In our experiments, we used both flat and vicinal Si(111) wafers as substrates. The vicinal substrates were tilted by either 0.5° or 1.1° toward the $[1\bar{1}2]$ direction (see fig. S1 in the Supplementary Materials). To create a SIC structure of Pb/Si(111), we initially prepared an atomically clean Si(111) 7-by-7 surface by outgassing at 600°C for several hours and flashing it at 1200°C multiple times. Subsequently, the SIC structure was formed by depositing 1.5 Ml of Pb on a clean Si(111) substrate at room temperature, followed by annealing at 358°C for 105 s. The resulting structure was confirmed by STM.

Surface electron transport measurements

For measuring the electrical conductance of the surface conductive layer, a four-terminal pattern with a probed area of 1.2 mm by 0.3 mm was created on the sample surface by Ar^+ sputtering through a shadow mask, as illustrated in fig. S2. The sample orientation was adjusted so that the current flowed along the $(1\bar{1}0)$ direction, which is parallel to the steps of the vicinal substrates (fig. S1A). Transport measurements were conducted in a ^3He -cooled ultrahigh-vacuum low-temperature system. To prevent current flow through the substrates, nondoped Si(111) ($\rho > 1000 \Omega\cdot\text{cm}$) was used. Resistance was calculated as the measured voltage divided by the bias current (1 μA). We confirmed that the current I_S is sufficiently low to avoid the enhancement of resistance with the increase in I_S (see text S2 for the detail). The dc resistance of the samples was measured using a nanovoltmeter (Keithley 2182A) with a dc bias current generated by a source meter (Keithley 2401) without filtering.

STM/S measurements

STM/S measurements were carried out at 0.36 K using a ^3He -cooled ultrahigh vacuum low-temperature scanning tunneling microscope (Unisoku USM-1300 with a Nanonis controller) equipped with a superconducting magnet capable of generating an out-of-plane magnetic field of up to 7 T. The tunneling conductance (dI/dV) spectra were acquired using a lock-in method with a modulation amplitude and frequency of a 30- μV peak and 971 Hz, respectively. Highly doped Si(111) substrates (As-doped, 1 to 3 $\text{m}\Omega\cdot\text{cm}$) were used for STM measurements.

Supplementary Materials

This PDF file includes:

Supplementary Text S1 to S7

Figs. S1 to S8

References

REFERENCES

1. G. Logvenov, A. Gozar, I. Bozovic, High-temperature superconductivity in a single copper-oxygen plane. *Science* **326**, 699–702 (2009).

2. A. T. Bollinger, G. Dubuis, J. Yoon, D. Pavuna, J. Misewich, I. Bozovic, Superconductor-insulator transition in $\text{La}_{2-x}\text{Sr}_x\text{CuO}_4$ at the pair quantum resistance. *Nature* **472**, 458–460 (2011).
3. J. M. Lu, O. Zheliuk, I. Leermakers, N. F. Q. Yuan, U. Zeitler, K. T. Law, J. T. Ye, Evidence for two-dimensional Ising superconductivity in gated MoS_2 . *Science* **350**, 1353–1357 (2015).
4. Y. Saito, Y. Kasahara, J. Ye, Y. Iwasa, T. Nojima, Metallic ground state in an ion-gated two-dimensional superconductor. *Science* **350**, 409–413 (2015).
5. Y. Saito, T. Nojima, Y. Iwasa, Quantum phase transitions in highly crystalline two-dimensional superconductors. *Nat. Commun.* **9**, 778 (2018).
6. X. Xi, Z. Wang, W. Zhao, J.-H. Park, K. T. Law, H. Berger, L. Forró, J. Shan, K. F. Mak, Ising pairing in superconducting NbSe_2 atomic layers. *Nat. Phys.* **12**, 139–143 (2015).
7. A. Tsen, B. Hunt, Y. Kim, Z. Yuan, S. Jia, R. Cava, J. Hone, P. Kim, C. Dean, A. Pasupathy, Nature of the quantum metal in a two-dimensional crystalline superconductor. *Nat. Phys.* **12**, 208–212 (2016).
8. S. Ichinokura, Y. Nakata, K. Sugawara, Y. Endo, A. Takayama, T. Takahashi, S. Hasegawa, Vortex-induced quantum metallicity in the mono-unit-layer superconductor NbSe_2 . *Phys. Rev. B* **99**, 220501 (2019).
9. T. Zhang, P. Cheng, W.-J. Li, Y.-J. Sun, G. Wang, X.-G. Zhu, K. He, L. Wang, X. Ma, X. Chen, Y. Wang, Y. Liu, H.-Q. Lin, J.-F. Jia, Q.-K. Xue, Superconductivity in one-atomic-layer metal films grown on Si(111). *Nat. Phys.* **6**, 104–108 (2010).
10. C. Brun, T. Cren, V. Cherkaz, F. Debontridder, S. Pons, D. Fokin, M. Tringides, S. Bozhko, L. Ioffe, B. Altshuler, D. Roditchev, Remarkable effects of disorder on superconductivity of single atomic layers of lead on silicon. *Nat. Phys.* **10**, 444–450 (2014).
11. A. Stępnik, A. Leon Vanegas, M. Caminal, H. Oka, D. Sander, J. Kirschner, Atomic layer superconductivity. *Surf. Interface Anal.* **46**, 1262–1267 (2014).
12. S. Yoshizawa, H. Kim, T. Kawakami, Y. Nagai, T. Nakayama, X. Hu, Y. Hasegawa, T. Uchihashi, Imaging Josephson vortices on the surface superconductor Si(111)–($\sqrt{7}\times\sqrt{3}$)–In using a scanning tunneling microscope. *Phys. Rev. Lett.* **113**, 247004 (2014).
13. S. Yoshizawa, H. Kim, Y. Hasegawa, T. Uchihashi, Disorder-induced suppression of superconductivity in the Si(111)–($\sqrt{7}\times\sqrt{3}$)–In surface: Scanning tunneling microscopy study. *Phys. Rev. B* **92**, 041410 (2015).
14. S. Ichinokura, L. Bondarenko, A. Tupchaya, D. Gruznev, A. Zotov, A. Saranin, S. Hasegawa, Superconductivity in thallium double atomic layer and transition into an insulating phase intermediated by a quantum metal state. *2D Materials* **4**, 025020 (2017).
15. F. Oguro, Y. Sato, K. Asakawa, M. Haze, Y. Hasegawa, Enhanced critical magnetic field for monoatomic-layer superconductor by Josephson junction steps. *Phys. Rev. B* **103**, 085416 (2021).
16. Y. Sato, M. Haze, R. Nemoto, W. Qian, S. Yoshizawa, T. Uchihashi, Y. Hasegawa, Squeezed Abrikosov-Josephson vortex in atomic-layer Pb superconductors formed on vicinal Si(111) substrates. *Phys. Rev. Lett.* **130**, 106002 (2023).
17. D. S. Baranov, S. Vlaic, J. Baptista, E. Cofler, V. S. Stolyarov, D. Roditchev, S. Pons, Gold atoms promote macroscopic superconductivity in an atomic monolayer of Pb on Si(111). *Nano Lett.* **22**, 652–657 (2022).
18. D. J. Bishop, E. G. Spencer, R. C. Dynes, The metal-insulator transition in amorphous Nb:Si. *Solid-State Electron.* **28**, 73–79 (1985).
19. B. G. Orr, H. M. Jaeger, A. M. Goldman, Local superconductivity in ultrathin Sn films. *Phys. Rev. B* **32**, 7586–7589 (1985).
20. D. Haviland, Y. Liu, A. M. Goldman, Onset of superconductivity in the two-dimensional limit. *Phys. Rev. Lett.* **62**, 2180–2183 (1989).
21. A. F. Hebard, M. A. Paalanen, Magnetic-field-tuned superconductor-insulator transition in two-dimensional films. *Phys. Rev. Lett.* **65**, 927–930 (1990).
22. H. M. Jaeger, D. B. Haviland, B. G. Orr, A. M. Goldman, Onset of superconductivity in ultrathin granular metal films. *Phys. Rev. B* **40**, 182–196 (1989).
23. S. Okuma, T. Terashima, N. Kokubo, Anomalous magnetoresistance near the superconductor-insulator transition in ultrathin films of $\alpha\text{-Mo}_2\text{Si}_{1-x}$. *Phys. Rev. B* **58**, 2816–2819 (1998).
24. N. Marković, C. Christiansen, A. M. Goldman, Thickness-magnetic field phase diagram at the superconductor-insulator transition in 2D. *Phys. Rev. Lett.* **81**, 5217–5220 (1998).
25. A. Frydman, The superconductor insulator transition in systems of ultrasmall grains. *Physica C* **391**, 189–195 (2003).
26. C. Christiansen, L. M. Hernandez, A. M. Goldman, Evidence of collective charge behavior in the insulating state of ultrathin films of superconducting metals. *Phys. Rev. Lett.* **88**, 037004 (2002).
27. T. I. Baturina, A. Y. Mironov, V. Vinokur, M. Baklanov, C. Strunk, Localized superconductivity in the quantum-critical region of the disorder-driven superconductor-insulator transition in TiN thin films. *Phys. Rev. Lett.* **99**, 257003 (2007).
28. C. Brun, T. Cren, D. Roditchev, Review of 2D superconductivity: The ultimate case of epitaxial monolayers. *Supercond. Sci. Technol.* **30**, 013003 (2017).
29. C. D. Chen, P. Delsing, D. B. Haviland, Y. Harada, T. Claeson, Scaling behavior of the magnetic-field-tuned superconductor-insulator transition in two-dimensional Josephson-junction arrays. *Phys. Rev. B* **51**, 15645–15648 (1995).

30. A. J. Rimberg, T. R. Ho, C. Kurdak, J. Clarke, Dissipation-driven superconductor-insulator transition in a two-dimensional Josephson-Junction array. *Phys. Rev. Lett.* **78**, 2632–2635 (1997).
31. M. P. Fisher, Quantum phase transitions in disordered two-dimensional superconductors. *Phys. Rev. Lett.* **65**, 923–926 (1990).
32. A. E. White, R. C. Dynes, J. P. Garno, Destruction of superconductivity in quench-condensed two-dimensional films. *Phys. Rev. B* **33**, 3549–3552 (1986).
33. A. Yazdani, A. Kapitulnik, Superconducting-insulating transition in two-dimensional a-MoGe thin films. *Phys. Rev. Lett.* **74**, 3037–3040 (1995).
34. D. Ephron, A. Yazdani, A. Kapitulnik, M. R. Beasley, Observation of quantum dissipation in the vortex state of a highly disordered superconducting thin film. *Phys. Rev. Lett.* **76**, 1529–1532 (1996).
35. T. Uchihashi, Two-dimensional superconductors with atomic-scale thickness. *Supercond. Sci. Technol.* **30**, 013002 (2017).
36. K. Ienaga, T. Hayashi, Y. Tamoto, S. Kaneko, S. Okuma, Quantum criticality inside the anomalous metallic state of a disordered superconducting thin film. *Phys. Rev. Lett.* **125**, 257001 (2020).
37. B. Sacépé, M. Feigel'man, T. M. Klapwijk, Quantum breakdown of superconductivity in low-dimensional materials. *Nat. Phys.* **16**, 734–746 (2020).
38. C. G. L. Böttcher, F. Nichele, M. Kjaergaard, H. J. Suominen, J. Shabani, C. J. Palmström, C. M. Marcus, Superconducting, insulating and anomalous metallic regimes in a gated two-dimensional semiconductor–superconductor array. *Nat. Phys.* **14**, 1138–1144 (2018).
39. C. H. Sharma, A. P. Surendran, S. S. Varma, M. Thalakulam, 2D superconductivity and vortex dynamics in 1T-MoSe₂. *Commun. Phys.* **1**, 90 (2018).
40. C. Yang, Y. Liu, Y. Wang, L. Feng, Q. He, J. Sun, Y. Tang, C. Wu, J. Xiong, W. Zhang, X. Lin, H. Yao, H. Liu, G. Fernandes, J. Xu, J. M. Valles Jr., J. Wang, Y. Li, Intermediate bosonic metallic state in the superconductor-insulator transition. *Science* **366**, 1505–1509 (2019).
41. Y. Xing, P. Yang, J. Ge, J. Yan, J. Luo, H. Ji, Z. Yang, Y. Li, Z. Wang, Y. Liu, F. Yang, P. Qiu, C. Xi, M. Tian, Y. Liu, X. Lin, J. Wang, Extrinsic and intrinsic anomalous metallic states in transition metal dichalcogenide Ising superconductors. *Nano Lett.* **21**, 7486–7494 (2021).
42. C. Yang, H. Liu, Y. Liu, J. Wang, D. Qiu, S. Wang, Y. Wang, Q. He, X. Li, P. Li, Y. Tang, J. Wang, X. C. Xie, J. M. Valles Jr., J. Xiong, Y. Li, Signatures of a strange metal in a bosonic system. *Nature* **601**, 205–210 (2022).
43. K. Ienaga, Y. Tamoto, M. Yoda, Y. Yoshimura, T. Ishigami, S. Okuma, Broadened quantum critical ground state in a disordered superconducting thin film. *Nat. Commun.* **15**, 2388 (2024).
44. E. Shimshoni, A. Auerbach, A. Kapitulnik, Transport through quantum melts. *Phys. Rev. Lett.* **80**, 3352–3355 (1998).
45. D. Das, S. Doniach, Existence of a Bose metal at $T=0$. *Phys. Rev. B* **60**, 1261–1275 (1999).
46. A. Kapitulnik, N. Mason, S. A. Kivelson, S. Chakravarty, Effects of dissipation on quantum phase transitions. *Phys. Rev. B* **63**, 125322 (2001).
47. D. Dalidovich, P. Phillips, Phase glass is a Bose metal: A new conducting state in two dimensions. *Phys. Rev. Lett.* **89**, 027001 (2002).
48. P. Phillips, D. Dalidovich, The elusive Bose metal. *Science* **302**, 243–247 (2003).
49. P. W. Phillips, Not just a phase. *Nat. Phys.* **12**, 206–207 (2016).
50. Y. Noat, V. Cherkez, C. Brun, T. Cren, C. Carillet, F. Debontridder, K. Ilin, M. Siegel, A. Semenov, H.-W. Hübers, D. Roditchev, Unconventional superconductivity in ultrathin superconducting NbN films studied by scanning tunneling spectroscopy. *Phys. Rev. B* **88**, 014503 (2013).
51. I. Roy, R. Ganguly, H. Singh, P. Raychaudhuri, Robust pseudogap across the magnetic field driven superconductor to insulator-like transition in strongly disordered NbN films. *Eur. Phys. J. B* **92**, 49 (2019).
52. S. Dutta, J. Jesudasan, P. Raychaudhuri, Magnetic field induced transition from a vortex liquid to Bose metal in ultrathin a-MoGe thin film. *Phys. Rev. B* **105**, L140503 (2022).
53. K. Horikoshi, X. Tong, T. Nagao, S. Hasegawa, Structural phase transitions of Pb-adsorbed Si (111) surfaces at low temperatures. *Phys. Rev. B* **60**, 13287–13290 (1999).
54. M. Yamada, Y. Sato, M. Haze, Y. Hasegawa, Simple model for striped-incommensurate phase formed by Pb adsorption on Si(111). *e-J. Surf. Sci. Nanotechnol.* **23**, 199–206 (2025).
55. R. S. Thompson, Microwave, flux flow, and fluctuation resistance of dirty type-II superconductors. *Phys. Rev. B* **1**, 327–333 (1970).
56. A. Larkin, A. Varlamov, *Theory of Fluctuations in Superconductors* (Clarendon, 2005).
57. J. Homoth, M. Wenderoth, T. Druga, L. Winking, R. Ulbrich, C. Bobisch, B. Weyers, A. Bannani, E. Zubkov, A. Bernhart, M. R. Kaspers, R. Möller, Electronic transport on the nanoscale: ballistic transmission and Ohm's law. *Nano Lett.* **9**, 1588–1592 (2009).
58. I. Matsuda, M. Ueno, T. Hirahara, R. Hobara, H. Morikawa, C. Liu, S. Hasegawa, Electrical resistance of a monatomic step on a crystal surface. *Phys. Rev. Lett.* **93**, 236801 (2004).
59. C. Tegenkamp, Z. Kallassy, H. Pfür, H. L. Gunter, Y. Zielasek, M. Henzler, Switching between one and two dimensions: Conductivity of Pb-induced chain structures on Si(557). *Phys. Rev. Lett.* **95**, 176804 (2005).
60. V. L. Berezinskii, Destruction of long-range order in one-dimensional and two-dimensional systems possessing a continuous symmetry group. II. Quantum systems. *Sov. Phys. JETP* **34**, 610–616 (1972).
61. J. M. Kosterlitz, D. J. Thouless, Ordering, metastability and phase transitions in two-dimensional systems. *J. Phys. C Solid State Phys.* **6**, 1181–1203 (1973).
62. R. C. Dynes, V. Narayanamurti, J. P. Garno, Direct measurement of quasiparticle-lifetime broadening in a strong-coupled superconductor. *Phys. Rev. Lett.* **41**, 1509–1512 (1978).
63. B. L. Altshuler, A. G. Aronov, Zero bias anomaly in tunnel resistance and electron-electron interaction. *Solid State Commun.* **30**, 115–117 (1979).
64. B. L. Altshuler, A. G. Aronov, P. A. Lee, Interaction effects in disordered Fermi systems in two dimensions. *Phys. Rev. Lett.* **44**, 1288–1291 (1980).
65. C. Carillet, V. Cherkez, M. Skvortsov, M. Feigel'man, F. Debontridder, L. Ioffe, V. Stolyarov, K. Ilin, M. Siegel, C. Noûs, Spectroscopic evidence for strong correlations between local superconducting gap and local Altshuler-Aronov density of states suppression in ultrathin NbN films. *Phys. Rev. B* **102**, 024504 (2020).
66. B. Sacépé, T. Dubouchet, C. Chapelier, M. Sanquer, M. Ovadia, D. Shahar, M. Feigel'man, L. Ioffe, Localization of preformed Cooper pairs in disordered superconductors. *Nat. Phys.* **7**, 239–244 (2011).
67. P. H. Kes, J. Aarts, J. van den Berg, C. J. van der Beek, J. A. Mydosh, Thermally assisted flux flow at small driving forces. *Supercond. Sci. Technol.* **1**, 242–248 (1989).
68. I. Guillamón, H. Suderow, A. Fernández-Pacheco, J. Sesé, R. Córdoba, J. M. De Teresa, M. R. Ibarra, S. Vieira, Direct observation of melting in a two-dimensional superconducting vortex lattice. *Nat. Phys.* **5**, 651–655 (2009).
69. J. Bardeen, M. J. Stephen, Theory of the motion of vortices in superconductors. *Phys. Rev.* **140**, A1197–A1207 (1965).
70. I. Tamir, A. Benyamini, E. J. Telford, F. Gorniaczyk, A. Doron, T. Levinson, D. Wang, F. Gay, B. Sacépé, J. Hone, K. Watanabe, T. Taniguchi, C. R. Dean, A. N. Pasupathy, D. Shahar, Sensitivity of the superconducting state in thin films. *Sci. Adv.* **5**, eaau3826 (2019).
71. A. Banerjee, A. Mohapatra, R. Ganesan, P. S. A. Kumar, Restoring superconductivity in the quantum metal phase of NbSe₂ using dissipative coupling. *Nano Lett.* **19**, 1625–1631 (2019).
72. S. Dutta, I. Roy, S. Mandal, J. Jesudasan, V. Bagwe, P. Raychaudhuri, Extreme sensitivity of the vortex state in a-MoGe films to radio-frequency electromagnetic perturbation. *Phys. Rev. B* **100**, 214518 (2019).
73. S. Ullah, A. T. Dorsey, Critical fluctuations in high-temperature superconductors and the Ettingshausen effect. *Phys. Rev. Lett.* **65**, 2066–2069 (1990).
74. N. Werthamer, E. Helfand, P. Hohenberg, Temperature and purity dependence of the superconducting critical field, H_{c2} . III. Electron spin and spin-orbit effects. *Phys. Rev.* **147**, 295–302 (1966).
75. Y. Xing, H.-M. Zhang, H.-L. Fu, H. Liu, Y. Sun, J.-P. Peng, F. Wang, X. Lin, X.-C. Ma, Q.-K. Xue, J. Wang, X. C. Xie, Quantum Griffiths singularity of superconductor-metal transition in Ga thin films. *Science* **350**, 542–545 (2015).
76. S. Okuma, S. Togo, M. Morita, Enhancement of the quantum-liquid phase by increased resistivity in thick a-Mo_{1-x}Si_x films. *Phys. Rev. Lett.* **91**, 067001 (2003).
77. Y. Dubi, Y. Meir, Y. Avishai, Nature of the superconductor-insulator transition in disordered superconductors. *Nature* **449**, 876–880 (2007).
78. S. Yoshizawa, T. Kobayashi, Y. Nakata, K. Yaji, K. Yokota, F. Komori, S. Shin, K. Sakamoto, T. Uchihashi, Atomic-layer Rashba-type superconductor protected by dynamic spin-momentum locking. *Nat. Commun.* **12**, 1462 (2021).
79. N. D. Mermin, H. Wagner, Absence of ferromagnetism or antiferromagnetism in one- or two-dimensional isotropic Heisenberg models. *Phys. Rev. Lett.* **17**, 1133–1136 (1966).
80. S. Coleman, There are no Goldstone bosons in two dimensions. *Commun. Math. Phys.* **31**, 259–264 (1973).
81. B. I. Halperin, D. R. Nelson, Resistive transition in superconducting films. *J. Low Temp. Phys.* **36**, 599–616 (1979).
82. M. R. Beasley, J. E. Mooij, T. P. Orlando, Possibility of vortex-antivortex pair dissociation in two-dimensional superconductors. *Phys. Rev. Lett.* **42**, 1165–1168 (1979).
83. M. V. Feigel'man, V. B. Geshkenbein, A. I. Larkin, Pinning and creep in layered superconductors. *Physica C* **167**, 177–187 (1990).

Acknowledgments: We thank K. Ienaga and Y. Kato for fruitful discussions. **Funding:** This work was partially supported by the Grants-in-Aid for Scientific Research (KAKENHI) from the Japan Society for the Promotion of Science grants JP18H01876 (to S.Y.), JP19H00859 (to Y.H.), JP20K15166 (to M.H.), JP20K20904 (to T.U.), JP21H01817 (to S.Y.), JP22H01961 (to T.U.), JP22KJ0920 (to Y.S.), JP22H00292 (to Y.H.), and JP22K14598 (to M.H.) and Support for Pioneering Research Initiated by the Next Generation (SPRING) supported by Japan Science and Technology Agency grant JPMJSP 2108 (to Y.S.). **Author contributions:** Conceptualization: Y.S., M.H., and Y.H. Methodology: Y.S., M.H., S.Y., T.U., and Y.H. Investigation: Y.S., M.H., R.N., W.Q., and S.Y. Funding acquisition: Y.S., M.H., S.Y., T.U., and Y.H. Supervision: T.U. and Y.H. Writing—original draft: Y.S., M.H., and Y.H. Writing—review and editing: Y.S., M.H., S.Y., T.U., and Y.H. **Competing interests:** The authors declare that they have no competing interests. **Data, code, and materials availability:** All data and code needed to evaluate and reproduce the results in the paper are present in the paper and/or the Supplementary Materials. This study did not generate new materials.

Submitted 4 December 2024

Accepted 19 February 2026

Published 20 March 2026

10.1126/sciadv.adu9610

Stable vortices in the anomalous metallic state observed on monoatomic-layer superconductors

Yudai Sato, Masahiro Haze, Ryohei Nemoto, Wenxuan Qian, Shunsuke Yoshizawa, Takashi Uchihashi, and Yukio Hasegawa

Sci. Adv. **12** (12), eadu9610. DOI: 10.1126/sciadv.adu9610

View the article online

<https://www.science.org/doi/10.1126/sciadv.adu9610>

Permissions

<https://www.science.org/help/reprints-and-permissions>

Use of this article is subject to the [Terms of service](#)

Science Advances (ISSN 2375-2548) is published by the American Association for the Advancement of Science. 1200 New York Avenue NW, Washington, DC 20005. The title *Science Advances* is a registered trademark of AAAS.

Copyright © 2026 The Authors, some rights reserved; exclusive licensee American Association for the Advancement of Science. No claim to original U.S. Government Works. Distributed under a Creative Commons Attribution License 4.0 (CC BY).